Lanthanide Doped V_2O_5/Al_2O_3 Catalysts: Structure−Activity Relationship in the SCR of NO_x†

M. A. Centeno,* P. Malet, I. Carrizosa, and J. A. Odriozola

Departamento de Química Inorgánica e Instituto de Ciencia de Materiales de Sevilla, Universidad de Sevilla-CSIC, Centro de Investigaciones Científicas Isla de la Cartuja, Avda. Americo Vespuccio s/n, 41092 Sevilla, Spain

Received: August 31, 1999; In Final Form: December 9, 1999

The structure of lanthanide-doped (La, Sm, and Ce) V_2O_5/Al_2O_3 catalysts for the Selective Catalytic Reduction (SCR) of NO_x with NH_3 in the presence of O_2 have been studied by means of XRD, S_{BET}, XAS, UV−vis, XPS, and TPR techniques. As function of the vanadium loading and lanthanide dopant used, an alteration of the electronic density of support cations and supported vanadium ions is detected. The activation energy of the catalysts in the SCR reaction is directly related with the Lewis acidity of the vanadium species, in such a way that the higher the ionicity of the V−O bond, the higher the specific activity of the catalysts.

Introduction

The selective catalytic reduction (SCR) of nitrogen oxides with ammonia is one of the most used processes to abate NO_x in flue gases. The main aspects of the SCR reaction are deeply reviewed.[1−4] Among the catalysts active in the SCR reaction, V_2O_5-based catalysts are the most active and selective. Supporting vanadia on an adequate support leads to an increase in the catalytic activity. The nature of the support being a key factor, because it influences the redox and acid−base properties of the solids, which determines their activity. Among the supports tested in the literature, γ-Al_2O_3 has been described as an appropriate one.[5,6]

On the other hand, the addition of lanthanide oxides to γ-Al_2O_3 hinders surface sinterization and modifies the electronic density of the aluminum atoms. Besides this, a modification of the electronic structure of the lanthanide cations also occurs. This charge redistribution over the AlOLn ensembles implies a modification of the acid−base properties of the support surface.[7,8] This change in the surface electronic structure of the solid is expected to produce a change in the catalyst activity.

In this paper, we present data someway related to those early obtained for one of us in Prof. G. Somorjai's laboratory.[9,10] Even though we have changed the catalyst and the characterization techniques, we did not forget his advice: *"if you are going to do catalysis, do it, do not just characterize solids."* Thus, we try to correlate the geometrical and electronic structure of V_2O_5/Al_2O_3 and lanthanide-doped (La, Sm, and Ce) V_2O_5/Al_2O_3 catalyst surfaces with the catalytic activity of the SCR reaction in order to understand how these factors can be managed for improving the catalyst efficiency.

Experimental Section

An impregnation method was followed for preparing 10 wt % Ln_2O_3/Al_2O_3 (Ln = Sm, La, Ce) supports. Adequate amounts of the lanthanide oxide (Sigma 99.9% pure) were dissolved in the smallest possible volume of 4 M HNO_3. Then, a slurry of γ-Al_2O_3 powder (Degussa, type C) in 200 mL of deionized water was added. The slurry thus prepared was taken into dryness by continuos stirring and heating (60−70 °C). The solid was then kept overnight at 120 °C in the oven, crushed in an agate mortar and calcined for 4 h at 600 °C. The Al_2O_3 support was subjected to the same process for comparative purposes.

In every case, the amounts of alumina and lanthanide oxide were chosen for obtaining 10% w/w Ln_2O_3/Al_2O_3 supports. This implies for the cerium doped support an 18.2% w/w CeO_2/Al_2O_3.

1%, 5%, and 10% w/w V_2O_5 loaded catalysts were prepared by impregnation. Stoichiometric amounts of ammonium metavanadate (NH_4VO_3, Merck, 99% pure) were dissolved in 20 mL of 1 M oxalic acid (Merck, 99.9% pure) solution, under continuous stirring and moderate heating to obtain the blue complex $(NH_4)_2[VO(C_2O_4)_2]$. Then, the support was added. The slurry was brought to dryness under continuos stirring at 80−100 °C. Finally, the solid was heated in air at 120 °C overnight, crushed in an agate mortar, and calcined at 500 °C for 6 h. We denote *x*VAl as the vanadia/alumina catalyst and *x*VLnAl (Ln = Sm, La, Ce) as the lanthanide doped ones, *x* being the weight percent of V_2O_5 of the samples.

TPR experiments were carried out in a conventional quartz reactor connected to a TCD. The reactive gas stream (5% H_2 in Ar) was flowed at 50 cm^3 min^{-1} and the temperature raised at 10 °C min^{-1}. A CO_2−acetone trap was used to condense the reduction products, mostly water. The weight of sample was calculated to get the *P* parameter to be below 20 K ($P = 5.5$ K), which ensures a differential regime and pseudo-order zero for hydrogen in the rate law of the process. This parameter was defined by Malet et al.[11] from the H_2 mass balance and the linear temperature program as

$$P = \frac{\beta S_o}{F C_o}$$

where β is the heating rate, S_o the initial amount of reducible species, *F* the carrier flow rate, and C_o the hydrogen concentration in the reaction mixture. For low *P* values, the hydrogen uptake is low with respect to the hydrogen feed to the reactor, and in these conditions, these authors reported a good resolution and the absence of distortions in the TPR profiles. Quantitative analysis was done by integration of the reduction signal and comparison with hydrogen consumption of a CuO reference.

† Part of the special issue "Gabor Somorjai Festschrift".

* Corresponding author. Phone: +34 5 4489544. Fax: +34 5 4460665. E-mail: centeno@cica.es.

10.1021/jp993084a CCC: $19.00
Published on Web 02/26/2000

All the gases employed had a purity of 99.998% (Sociedad Española del Oxígeno, SEO) and were used without further purification.

XRD analysis was performed in a Siemens Krystalloflex D-500 X-ray diffractometer by using Cu K_α radiation and pyrolytic graphite as a monochromator and standard recording conditions, the detection limit of the technique being about 5 nm.

The specific surface area was measured by the single-point BET method in a Micromeritics Flowsorb II 2300 apparatus. Before analysis, samples were degassed for 3 h at 250 °C under nitrogen flow.

Diffuse reflectance UV−vis spectra were recorded at room temperature on a Shimadzu UV-2101PC spectrometer equipped with an integrating sphere and using in each series of vanadium catalysts, the corresponding support as reference.

X-ray photoelectron spectra (XPS) were collected in a Vacuum Generator 210 spectrometer working at 30 eV constant pass energy at a pressure around 3×10^{-10} Torr. Mg Kα at 240 W was used as an excitation radiation. Samples were outgassed during 12 h at room temperature in a pretreatment chamber at 10^{-7} Torr base pressure before being introduced in the analysis chamber. The binding energies were calculated with respect to the C−(C−H) component of the C 1s adventitious carbon fixed at 284.6 eV.

Room-temperature XAS spectra were recorded in transmission mode at the V-K and Sm-L_{III} edges at LURE DCI storage ring (Orsay, France). The overlap of the V-K and La-L_{III} edges prevents the analysis of the lanthanum-doped samples. Also, the low-energy gap between the V-K and Ce-L_{III} edges (200 eV) makes only the XANES analysis of the cerium-doped samples reliable. Monochromatization was achieved with a double silicon crystal working at the (311) reflection and detuned to an 80% of its maximum intensity to avoid higher harmonics. The measurements were carried out in transmission mode using optimized ion chambers as detectors. Samples were placed on Kapton Sellotape with an absorbance of ca. 2.5 ($\Delta\mu_x < 1$) just above the absorption edge. Analysis and handling of the EXAFS spectra were carried out by using the code NEWEXAFS from the Eindhoven University of Technology. This program uses standard procedures to extract the EXAFS spectra from the measured absorption data.[12] Absolute energies were calibrated by setting the first peak in the derivative XAS spectrum of a V foil at 5465.2 eV. EXAFS data were analyzed by multiple-shell fitting in k and R spaces using phase shifts and backscattering amplitudes for V−O obtained from Na_3VO_4 spectrum ($\lambda = 1.69$ Å; oxygen coordination number of vanadium ions = 4).[13] Standard deviations of fitted parameters were calculated for a mean noise level of 5×10^{-4}. Estimated systematic errors in bond distances, R (±1−3%), and coordination numbers, N (±10−15%), are in general higher than the calculated standard deviations. White line intensities have been measured after normalization of the XANES spectra using the procedure previously described by us.[7,8,14]

A catalytic test was carried out in a continuous flow reactor working at atmospheric pressure and integral reactor conditions. 3000 ppm of NO in N_2 (Abello Oxigeno Linde), 3000 ppm of NH_3 in N_2 (Abello Oxigeno Linde), and synthetic air (Sociedad Española del Oxigeno (SEO, 99.999% pure) were used as reactants. The experimental reaction conditions are shown in Table 1.

Before the reaction, the catalyst was activated at 500 °C for 2 h in 20 mL min^{-1} of synthetic air. Then, the SCR feed was admitted into the reactor. NO concentration outlet of the reactor was monitored by a gas electrochemical analyzer LANCOM 6500. Activity results were taken after 1 h in reaction at every temperature, even though the steady state was reached after 30 min in stream. The reactor showed no activity under these conditions.

TABLE 1: SCR Experimental Conditions

nitric oxide (NO)	1000 ppm
ammonia (NH_3)	1000 ppm
oxygen (O_2)	1%
nitrogen (N_2)	balance
temperature	150−500 °C
pressure	atmospheric
catalysts weight	200 mg
total flow	60 mL min^{-1}

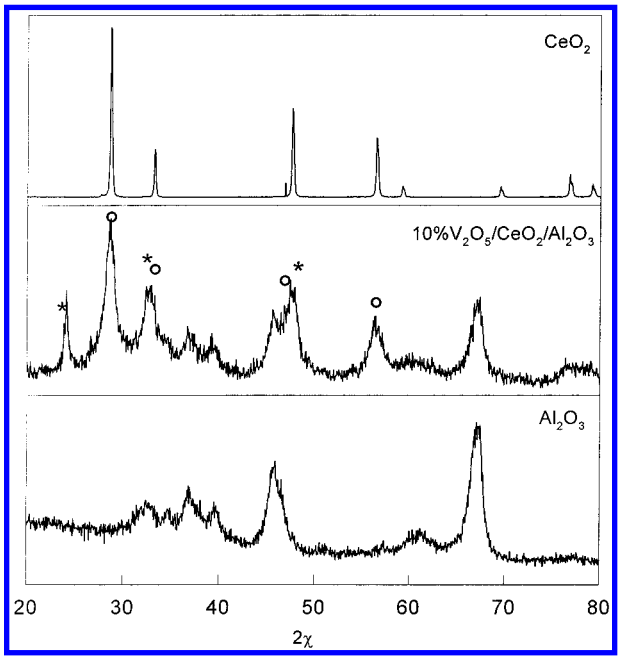

Figure 1. XRD pattern of 10VCeAl catalyst and reference compounds CeO_2, Al_2O_3, and $CeVO_4$. (*) and (○) indicate the peaks assigned to $CeVO_4$ and CeO_2, respectively.

Results and Discussion

Catalysts. All the catalysts synthesized present the same specific surface BET area of the starting support (82 ± 5 m^2 g^{-1}). Taking into account this surface area and the estimated area occupied by a $VO_{2.5}$ unit (1.05×10^{-19} m^2), the number of theoretical monolayers of vanadium oxide on the support was calculated to be 0.08, 0.42, and 0.85 for the solids with, respectively, 1%, 5%, and 10% w/w of V_2O_5.

XRD patterns of all supports and low loaded vanadium catalysts (<10%) present only peaks due to γ-Al_2O_3. In addition, peaks of CeO_2 are also detected in cerium-doped samples. For the highest loaded vanadium catalysts (10% w/w), a weak peak is detected at 27° in the case of 10VLaAl and 10VSmAl that could be ascribed to vanadate-like species.[15] The low intensity of this peak and the absence of new crystalline phases associated with vanadium can be explained either by the low concentration of such vanadate species or/and by assuming that they are very dispersed on the catalysts surface. 10VCeAl solid presents clearly peaks of $CeVO_4$ (Figure 1). The formation of such cerium vanadate has been detected in V_2O_5/CeO_2 catalysts with a vanadium molar content higher than 5%,[16] suggesting that the presence of high amounts of vanadium ions induces the reduction of part of the cerium (IV) ions to cerium (III).

XAS Analysis. Figure 2 shows the EXAFS oscillations at the V K-edge and their associated Fourier transforms of the

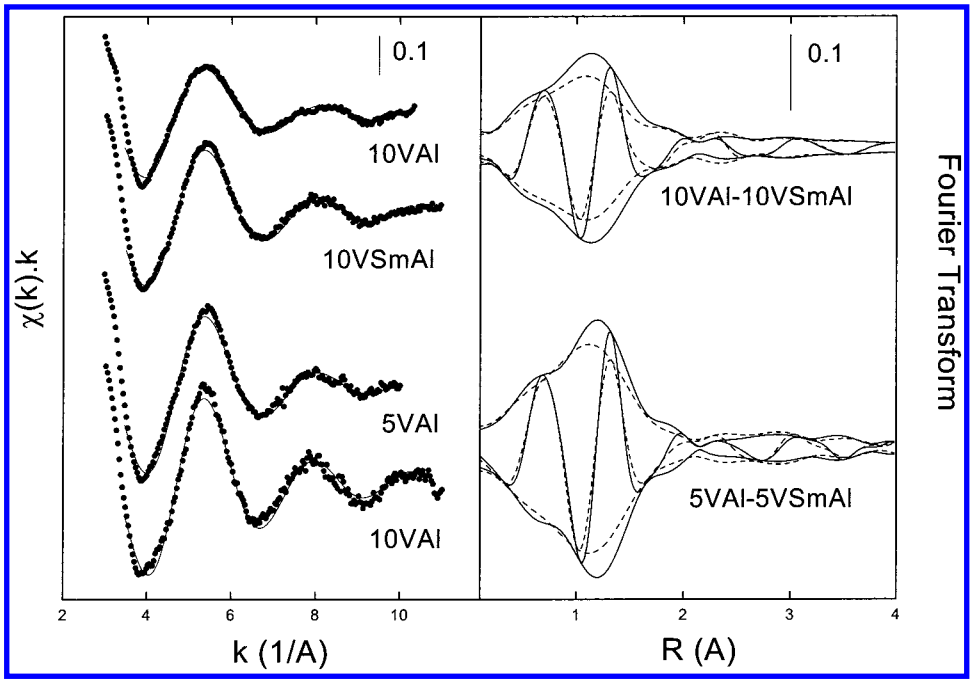

Figure 2. (left) Raw EXAFS oscillations at the V K-edge (●) and best-fit functions (lines) of high vanadium loaded catalysts. (right) Experimental k^1-FTs (dash lines, undopped; solid lines, Sm-doped, $\Delta k = 3-10$ Å^{-1}).

TABLE 2: EXAFS Parameters and Standard Deviations for V_2O_5/Al_2O_3 and Sm-Doped V_2O_5/Al_2O_3 Samples

sample	shell	N	$\Delta\sigma^2$ (Å^2)·10^{-3}	R (Å)	$\Delta E°$ (eV)
10VAl	O_1	2.7 ± 0.4	4.7 ± 0.9	1.62 ± 0.01	7 ± 2
	O_2	1.5 ± 0.6	14 ± 3	1.82 ± 0.02	5 ± 2
10VSmAl	O_1	3.1 ± 0.5	3.0 ± 0.9	1.63 ± 0.01	7 ± 1
	O_2	0.9 ± 0.6	14 ± 6	1.82 ± 0.06	5 ± 4
5VAl	O	4.17 ± 0.02	6.00 ± 0.07	1.634 ± 0.001	8.0 ± 1
5VSmAl	O	3.88 ± 0.01	1.96 ± 0.07	1.658 ± 0.001	4.4 ± 1

undopped and samarium-doped vanadium catalysts. Table 2 presents the best fit obtained for such oscillations using experimental phase shift and backscattering amplitude functions for V−O obtained from the spectra of Na_3VO_4. A regular tetrahedral coordination is found in the 5% V_2O_5 samples. A lower dispersion of V−O bond distances in the Sm-doped samples is suggested from the lower Debye−Waller factor obtained in the fit. For the 10% V_2O_5 samples, the one-shell model produces O/V coordination numbers that are too low and without physical meaning (3.1 ± 0.1), suggesting the presence of two different V−O distances. A fit with a two shells models leads to oxygen subshells at 1.62 ± 0.01 and 1.82 ± 0.02 Å, and a total coordination number of about 4. The fraction of oxygen atoms at the longest distance is smaller in the samarium-doped sample. From here, the tetrahedral coordination of vanadium atoms in all samples is deduced. The regular character of the [VO_4] tetrahedra is favored at low vanadium loading and when doping with samarium. At high vanadium loading, these tetrahedra become irregular, showing two V−O distances similar to that observed by Kozlowski et al. in V_2O_5/Al_2O_3 samples.[17]

XANES spectra at the V K-edge of the solids studied show an intense pre-edge peak characteristic of V^{5+} in nonoctahedral coordination.[18] The normalized intensity as well as the position of this pre-edge peak is dependent on the vanadium content and the presence of the lanthanide dopant (Figure 3). The prepeak intensity increases as the vanadium loading decreases and when the support is doped with lanthanide ions. This prepeak has been ascribed[18] to a strictly dipole forbidden 1s → 3d transition. If symmetry of the V absorber coordination polyhedron is lowered from O_h, the inversion center is broken and the transition is dipole allowed due to the overlap of V 3d orbitals with ligand 2p orbitals.[19] The prepeak intensity is expected to show the highest intensity for regular [VO_4] tetrahedra due to the lack of an inversion center in this polyhedron. The intensity of the pre-peak along the series of

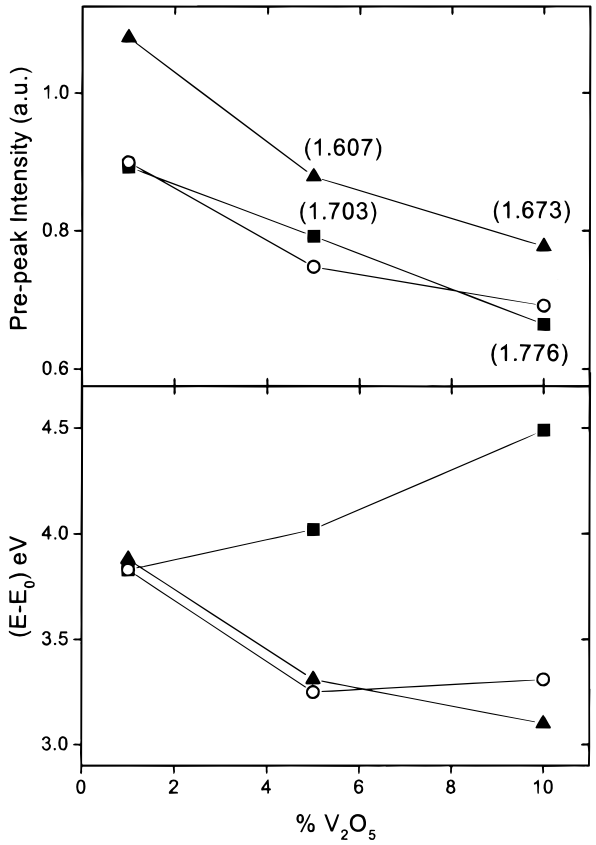

Figure 3. Normalized intensity and position of the V pre-edge peak for the catalysts considered, as a function of the V_2O_5 content. The prepeak position is calculated which respect to the first inflection point in the XAS spectrum of a vanadium foil, $E° = 5465.2$ eV: (■) undopped; (σ) Sm-doped; (○) Ce-doped. Numbers in brackets correspond to the average bond length, R.

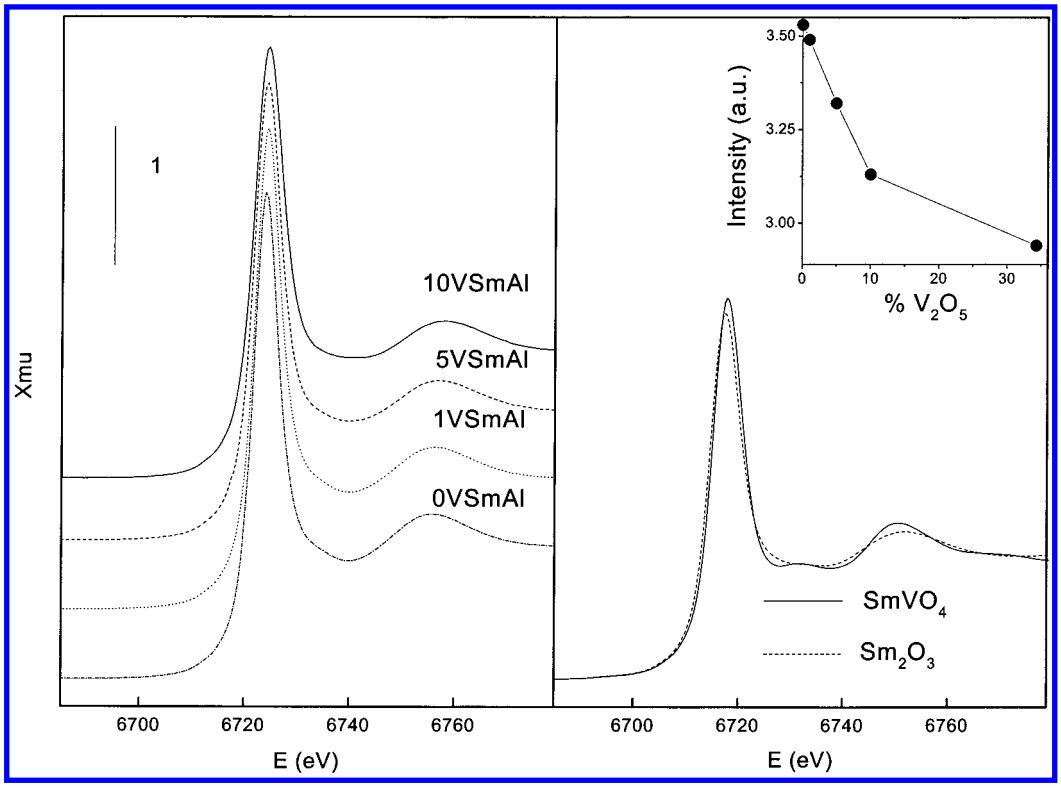

Figure 4. XANES spectra at the Sm-L_{III} edge of La-doped samples and reference compounds (Sm_2O_3 and $SmVO_4$). The white line intensity as a function of the vanadium content is presented in the figure inserted.

catalysts prepared might be ascribed to a linear combination of octahedral and tetrahedral sites for vanadium. However, on the basis of EXAFS data shown above, the presence of octahedral sites is disregarded. For a given geometry the intensity of the prepeak varies with the average bond length, $\bar{R}$, in such a way that the higher the average bond length the lower the prepeak intensity. Where $\bar{R}$ is defined by Wong et al.[18] as

$$\bar{R} = \frac{1}{n}\sum_{i=1}^{n} R_i$$

n being the coordination number and R_i the different V−O distances within the coordination polyhedron. Calculated average bond lengths are presented in Figure 3 showing a quite good correlation with the prepeak intensity.

The evolution observed in the intensity of the prepeak of the cerium-doped catalysts let us propose that the vanadium coordination environment is similar to that presented in undopped samples. On the other hand, the position of the prepeak shifts to higher energies when increasing the vanadium loading in the undopped samples while, for the lanthanide-doped ones, the shift is toward lower energies. As it has been described that a decrease in the electronic density on V 3d levels leads to a chemical shift of the prepeak to higher energies,[18] the behavior observed in the catalysts suggests that the ionicity of vanadium atoms increases as the vanadium loading increases when supported on undoped Al_2O_3, while the reverse is true when supported on lanthanide-doped one. In the cerium-doped series, a little change in the trends is observed for 10VCeAl, this behavior being ascribed to the presence of cerium vanadate, as stated by XRD measurements.

The XANES spectra at the Sm-L_{III} edge of the lanthanide-doped catalyst series (Figure 4) are dominated by a strong atomic absorption (white line) which corresponds to a Sm 2p → 5d transition,[20] its intensity depending on the electronic density of the Sm 5d levels. In the samples studied, the intensity of this white line is always higher than that of pure Sm_2O_3 and decreases continuously with the vanadium content. On the other hand, the intensity observed in the 10VSmAl catalyst is close to that of $SmVO_4$. The higher intensity of the white line of Sm_2O_3/Al_2O_3 support compared to that of Sm_2O_3 has been yet reported and explained in the basis of a electronic transference from the samarium ions to the aluminum cations, resulting in a decrease of the electronic density of the Sm 5d levels.[7] In accordance with this explanation, we must conclude that the addition of vanadium ions to the Sm_2O_3/Al_2O_3 support induces an increase in the electronic density of the Sm 5d levels. The resembling value observed for 10VSmAl and $SmVO_4$ could indicate the formation of surface $SmVO_4$ at high vanadium loading.

Figure 5 shows the XANES spectra at the Ce-L_{III} edge of the cerium-doped vanadium catalysts. Spectra are characterized by two peaks resulting from a charge transfer from O 2p orbitals to the cerium 4f states,[21−23] the peak at lower energy is associated with a $2p^54f^25d^1$ final state of Ce^{4+} ions, the shoulder at even lower energies corresponds to a $2p^54f^15d^1$ final state, while the peaks at higher energies are mainly due to a $2p^54f^0$-$5d^1$ final state.[24] Cerium trivalent compounds exhibit a single transition corresponding to the $2p^54f^15d^1$ final state configuration. The energy of this transition is identical to that of the shoulder in the low-energy region of Ce^{3+} compounds. When the vanadium content of the catalysts is increased, the lower energy peak broadens, increases in intensity, and shifts to lower energies, Figure 5. This can be related to a partial reduction of Ce(IV) to Ce(III). The relative intensity between the two peaks shown in the figure has been demonstrated by Malterra[23] to be proportional to the 4f orbitals population and hence is representative of the cerium oxidation state.

UV−Visible Experiments. Figure 6 shows the diffuse reflectance UV−vis spectra of the catalysts considered, taking

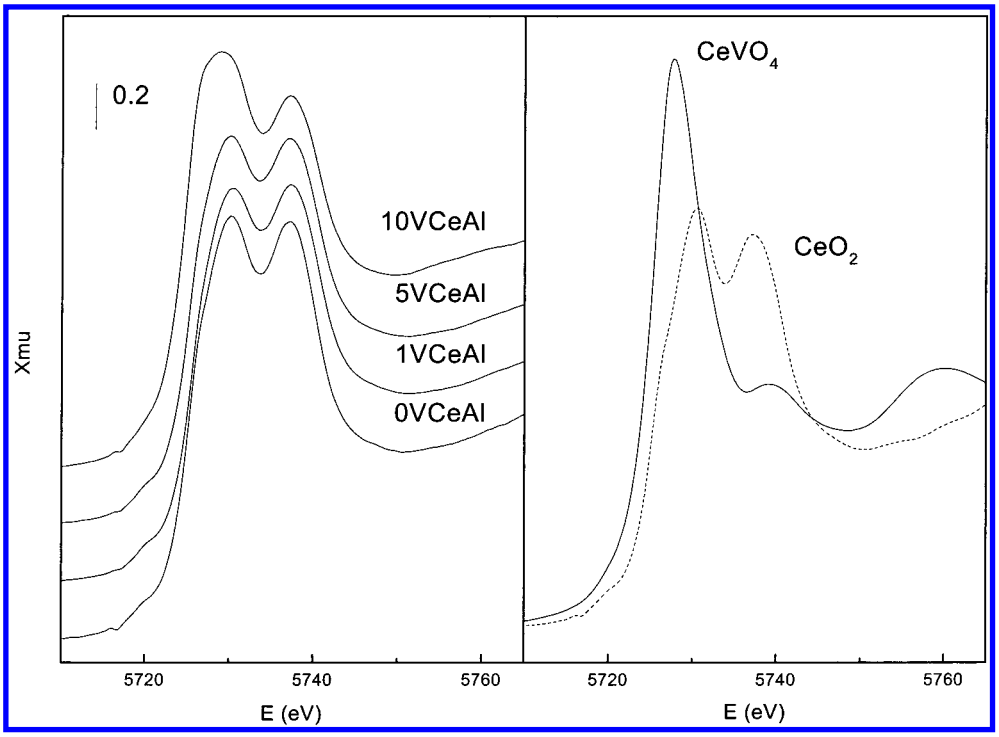

Figure 5. XANES spectra at the Ce-L_{III} edge of Ce-doped samples and reference compounds (CeO_2 and $CeVO_4$).

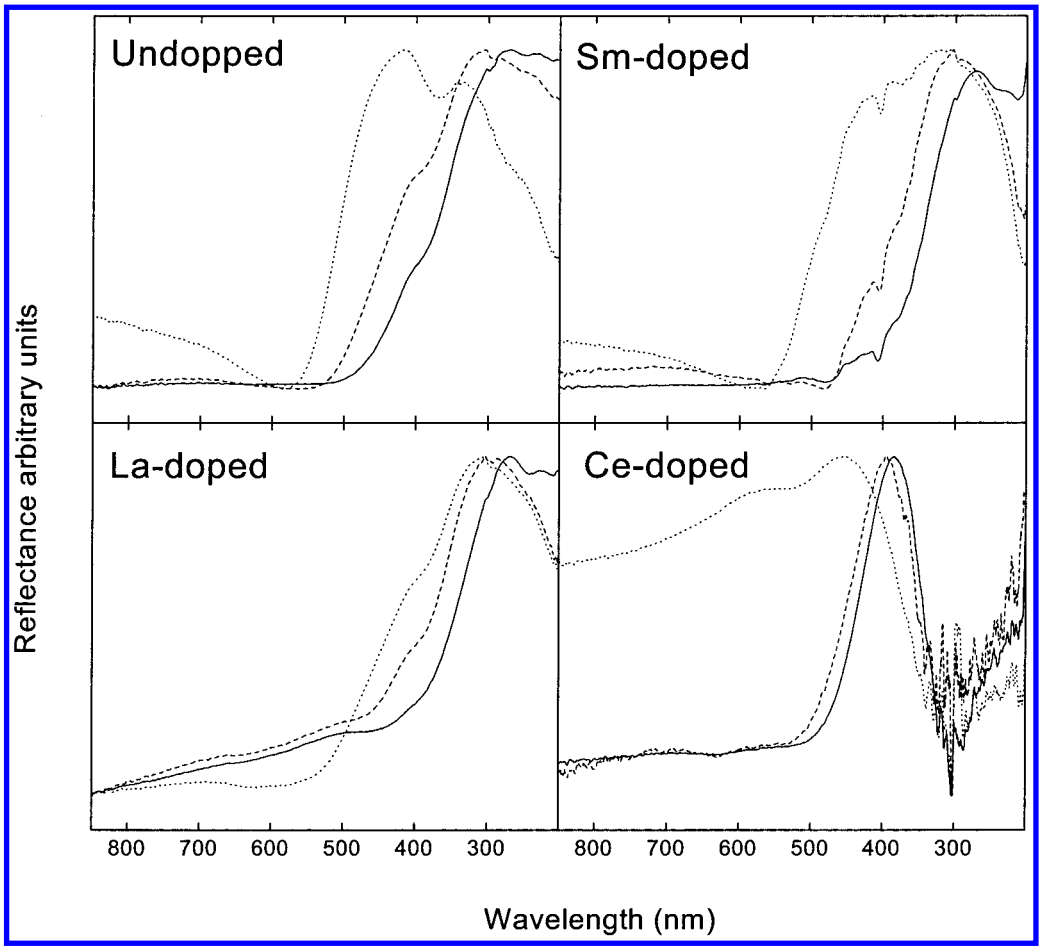

Figure 6. Normalized diffuse reflectance UV−vis spectra of the catalysts studied, taking the spectrum of the corresponding support as reference (solid lines, 1% V_2O_5; dash lines, 5% V_2O_5; dot lines, 10% V_2O_5).

the spectrum of the corresponding support as reference. Table 3 summarizes the positions of the absorption bands observed. The spectra of the solids with 1% w/w of vanadium present a wide band around 270 nm and a shoulder at higher wavelengths, ca. 400 nm, both characteristic of ligand charge-transfer (LCT) transitions of vanadium (V) species.[25,26] Increasing the vanadium content, a red-shift of the absorptions bands and a relative growing of the one at 400 nm are observed. This shift is due to

TABLE 3: Diffuse Reflectance UV−vis Absorption Bands of the Studied Catalysts

sample	$\%V_2O_5$	positions (nm)				
1VAl	1	275	400			
5VAl	5	305	410			600−800
10VAl	10	340	420			600−800
1VSmAl	1	270	400			
5VSmAl	5	305	410			600−800
10VSmAl	10	310	420			600−800
1VLaAl	1	270	400			
5VLaAl	5	290	410			600−800
10VLaAl	10	310	410			600−800
1VCeAl	1		385			
5VCeAl	5		395			600−800
10VCeAl	10			455	570	600−800

a considerable wideness of the bands more than a real change in the absorption maxima. The assignment for these bands in the literature is often made on the basis of changes in the coordination and/or polymerization degree of the vanadium atoms. The lower the coordination and polymerization, the lower the energy of the absorption band. Following these criteria, the absorption band around 270 nm could be ascribed to isolated monomeric tetrahedral vanadium species[25] and that around 400 nm to pentahedral ones.[27] The observed red shift when increasing the vanadium loading would be indicative of an increasing polymerization degree of such species, and the relative increment of the band at 400 nm would be indicative of an increase in the vanadium coordination. Another possible explanation arises from the XAS results. At low vanadium contents, a regular tetrahedral coordination of vanadium ions is observed in all series. Doping with lanthanide ions and increasing the vanadium content, a modification of the energy of the vanadium 1s → 3d transition is produced. This must be reflexed in a position shift of the UV−vis band absorptions. On the other hand, at high vanadium contents, the $[VO_4]$ polyhedra decrease in symmetry. The lower symmetry produces an increasing in the number of the allowed UV−vis transitions, widening the observed absorption bands.

On the other hand, a wide absorption in the 600−800 nm region, associated with d−d transitions of vanadium (IV) ions[26,28] is also observed for the high vanadium loaded catalysts.

Cerium-doped catalysts present a different behavior. At low vanadium loading, only one band due to vanadium (V) species in pentahedral coordination is observed, its position shifting from 385 to 395 nm when increasing the vanadium content from 1% to 5%. For the 10VCeAl catalysts, two absorptions bands at 455 and 570 nm are detected, the former characteristic of octahedral species and the latter indicative of the presence of a polymeric vanadate.[29] In fact, the detection of $CeVO_4$ by XRD measurement in this sample (Figure 1) confirms this assignation.

XPS Analysis. The O 1s, Al 2p, V 2p, and Ln (Sm, La, Ce) 3d levels have been recorded for all the catalysts, the supports and for comparative purposes, the ones of the $CeVO_4$ are also measured.

The V 2p binding energy of the lanthanide doped catalysts is constant and independent of the support nature (516.8 ± 0.1 eV) and coincides with that of the $CeVO_4$ sample. However, for the undopped catalysts, it shifts to higher binding energy (517.2 eV) with the vanadium content indicating a decrease in the electronic density of the vanadium ions. The O 1s binding energy remains constant at 531.0 ± 0.2 eV for all the studied solids.

The Al 2p binding energy remains constant, 74.0 ± 0.2 eV, with the support nature and vanadium loading. A detailed analysis could show a low increase in this value when increasing the vanadium content, this meaning an increase in the Lewis acidity of the aluminum cations when supporting vanadium.

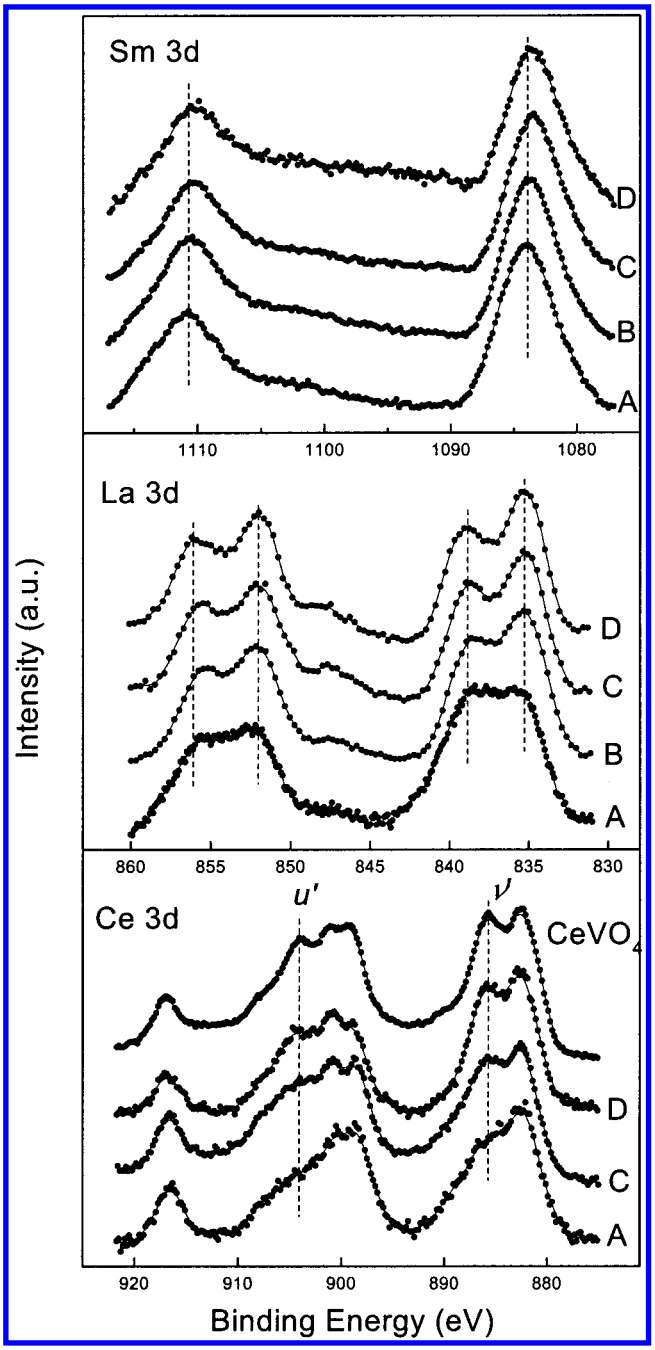

Figure 7. XPS spectra at Ln 3d regions (Ln = Sm, La, Ce) of the corresponding lanthanide-doped series of catalysts: (A) 0% V_2O_5; (B) 1% V_2O_5; (C) 5% V_2O_5; (D) 10% V_2O_5.

However, although the trend is clear, the difference between the limit values (≤0.3 eV) is not high enough to state it.

Figure 7 shows the Ln 3d (Ln = Sm, La, and Ce) XPS regions of the catalysts. In the samarium-doped series, the introduction of vanadium in the support produces a continuous decrease in the Sm 3d binding energy from 1083.9 for the samarium modified support to 1083.3 for the 10VsmAl catalyst. This means an increase in the electronic density of the samarium levels, in good agreement with the intensity variation observed in the white line of the XANES spectra at the Sm-L_{III} edge (Figure 4). For the lanthanum-doped series, neither the binding energy of the main La 3d peak (835.3 ± 0.2 eV) nor the distance between it and the associated satellite (3.5 eV) is modified with the introduction of vanadium. However, the relative intensity of the satellite decreases continuously with the vanadium loading. The modification of the relative intensity of satellite

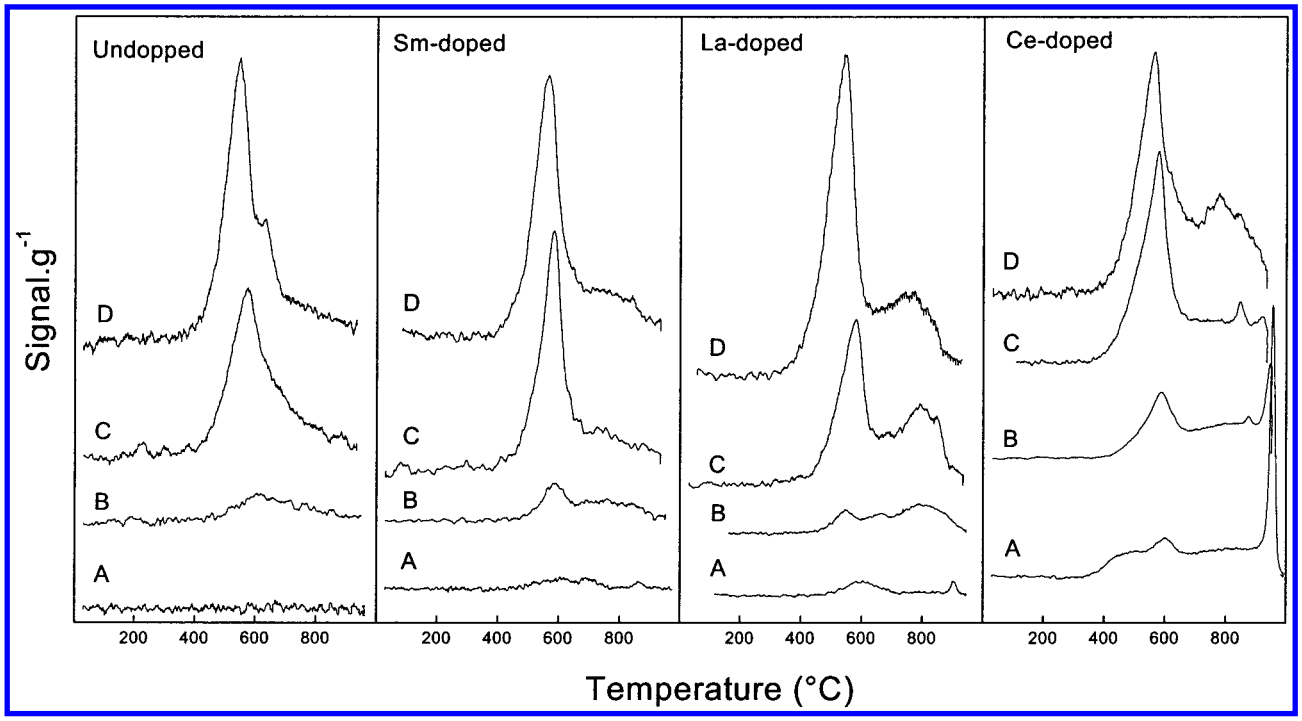

Figure 8. TPR profiles of the catalysts studied: (A) 0% V_2O_5; (B) 1% V_2O_5; (C) 5% V_2O_5; (D) 10% V_2O_5.

against the main La 3d peak has been previously observed in other systems containing lanthanum being ascribed to a change in the covalence of the La−O bond.[30] Thus, it must be related with a modification in the electronic density of lanthanum atoms when supporting vanadium. The complex shape of the 3d cerium spectra arises from several factors: multiplet effect, hybridization of Ce 4f orbitals with O 2p levels, and final state effects. Detailed discussions of these effects on the Ce 3d shape can be found in excellent reports.[24,31,32] In general, the same considerations are taken into account for discussing XAS and XPS spectra of cerium compounds except for the interaction between the photoelectron and the remaining system that cannot be neglected in XAS spectra.[23] The introduction of vanadium in the cerium-doped support produces a change in the Ce 3d XPS spectra from that characteristic of CeO_2 to that of $CeVO_4$, mainly consisting of the intensity increase of two features usually named v′ and u′ appearing at 885.8 and 903.9 eV, respectively. These lines are associated with $3d^94f^1V^n$ Ce(III) final states, where V^n represents the full valence band.[24,31] This intensity increases in addition with the modification of the L_{III} spectra suggests the reduction of the cerium (IV) atoms to cerium (III) on increasing the vanadium content.

Temperature-Programmed Reduction Study. The TPR profiles and hydrogen consumption of all samples are shown in Figure 8 and Table 4, respectively. The H_2 consumption of the supports increases in the sequence

$$Al_2O_3 < Sm_2O_3/Al_2O_3 < La_2O_3/Al_2O_3 < CeO_2/Al_2O_3$$

Cerium-doped support presents an H_2 consumption higher than necessary for the total reduction $Ce^{4+} \rightarrow Ce^{3+}$. This fact has been previously observed in cerium oxide and has been ascribed to dissolution of hydrogen atoms in the oxide network.[33] In the same sense, the hydrogen dissociation by rare earth oxides has been also described.[34]

In general, the TPR profile of the vanadium samples is characterized by an intense peak between 550 and 600 °C which shifts to lower temperature with the increasing vanadium content. Similar behavior has been early described for V_2O_5/Al_2O_3, and explained by the formation, at high vanadium loads, of vanadium polymeric species, which are more easily reducible than monomeric ones.[35] In this sense, the observed red shift of the UV−vis absorption bands and the more distorted [VO_4] tetrahedra detected by XAS when increasing the vanadium loading could support this explanation. On the other hand, the presence of vanadates (stated by XRD and XPS results) could have a similar effect. A second TPR peak at higher temperatures (770−850 °C) appears at high vanadium contents. In 10VCeAl, the appearance of this peak coincides with the simultaneous removing of the intense peak presents in the cerium-doped support at 955 °C, ascribed to the $Ce^{4+} \rightarrow Ce^{3+}$ reduction process.[36] The position of the peak matches with the one observed in $CeVO_4$. This observation allows us to assign the high-temperature peak to the reduction of vanadium atoms in vanadate-like compounds. It is important to note that the formation of $CeVO_4$ in 10VCeAl means that the presence of vanadium ions in large amounts induces the reduction of Ce(IV) ions to Ce(III) ones, even a room temperature.

The H_2 consumption of the undopped supported vanadium catalysts suggests an overall reduction to V^{4+}, according with previous bibliographic results over V_2O_5/Al_2O_3 catalysts.[37] In the case of $CeVO_4$, the reduction of vanadium ions continues

TABLE 4: Hydrogen Consumption in TPR Experiments

sample	H_2 consumption (μmol g^{-1})	H/V atomic ratio
0VAl	5.66	
1VAl	77.26	1.40
5VAl	445.64	1.62
10VAl	567.92	1.03
0VSmAl	37.66	
1VSmAl	137.64	2.50
5VSmAl	465.40	1.69
10VSmAl	625.94	1.14
0VLaAl	45.32	
1VLaAl	168.18	3.24
5VLaAl	658.09	2.39
10VLaAl	1182.46	2.15
0VCeAl	426.83	
1VCeAl	461.63	8.39
5VCeAl	665.09	2.42
10VCeAl	1182.46	2.15
$CeVO_4$	$4.55\ 10^3$	2.32

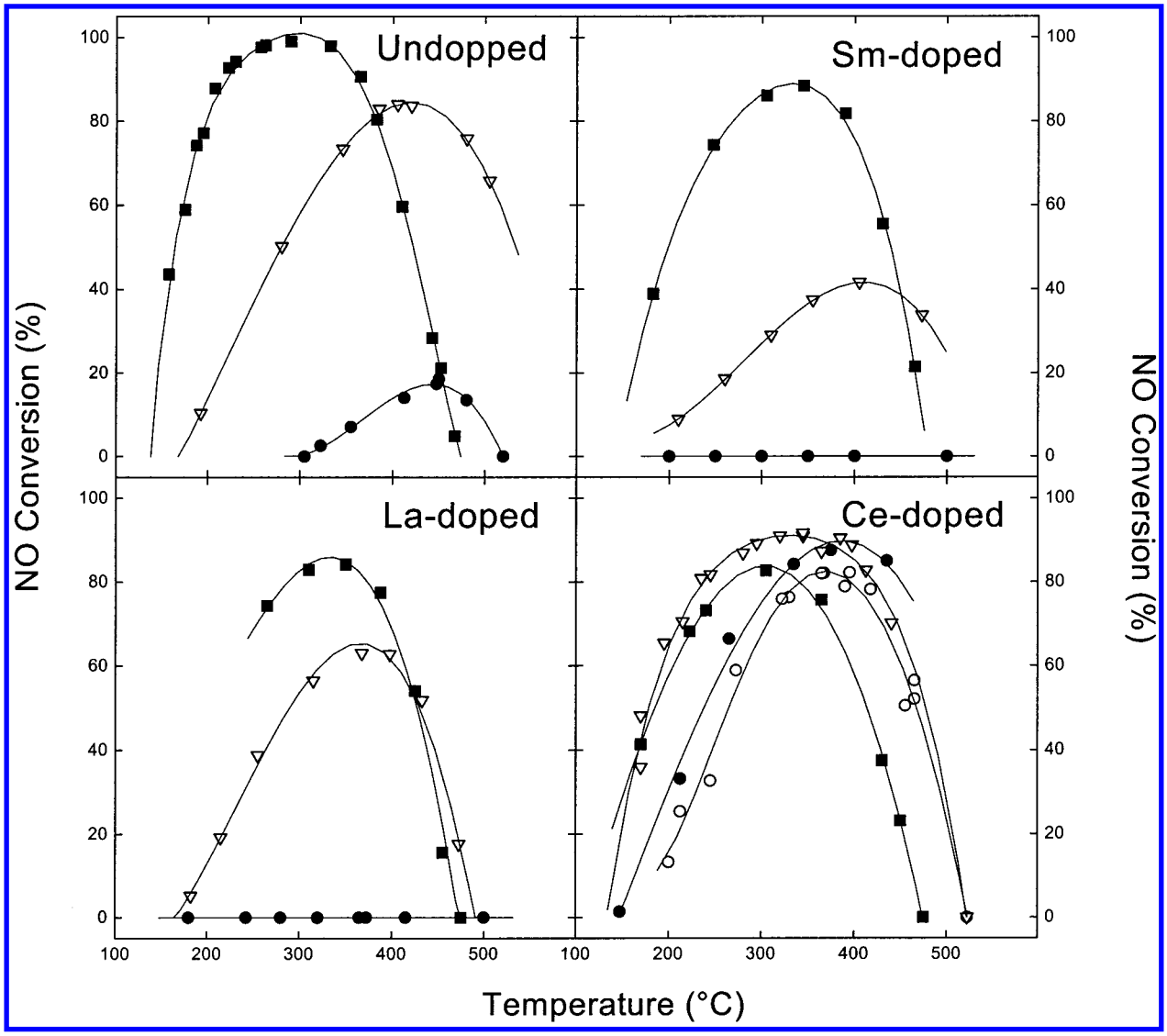

Figure 9. NO conversion (%) as a function of the temperature, for all the catalysts tested: (○) 0% V_2O_5; (●) 1% V_2O_5; (▽) 5% V_2O_5; (■) 10% V_2O_5.

until V^{3+}. The analysis of the H_2 consumption over the lanthanide-doped V_2O_5/Al_2O_3 catalysts is more complex, since we must take into account (i) the support ability to H_2 consummation, very important in the case of cerium-doped samples, (ii) the formation of lanthanide vanadates, trending to increase the H/V ratio to 2, and (iii) the reducibility of any other supported phase of vanadium.

Catalytic Reaction. All supports, except the cerium-doped one, show no activity, in good agreement with the bibliographic assessment of the absence of SCR activity of γ-Al_2O_3.[37−39] However, the cerium-doped γ-Al_2O_3 sample presents an important NO conversion. In this case, the activity must be related with the existence of the redox pair Ce^{3+}/Ce^{4+} which it has been described to be an effective active site for the SCR reaction.[40,41]

Figure 9 shows the evolution of the NO conversion with the reaction temperature over the studied catalysts. Two competing reactions occur under the conditions employed: reduction of nitric oxide by ammonia and oxidation of ammonia by oxygen. At low temperatures, the former reaction is predominant and the latter becomes the major reaction at high temperatures. According to it, NO conversion passes in every case through a maximum being the decrease observed due to consumption of ammonia by independent oxidation. In all series of catalysts, NO conversion increases with the vanadium content. This is in agreement with literature data that describes the maximum activity in the SCR of NO_x for V_2O_5 based catalysts, for V_2O_5 contents between 10% and 20%.[42] The introduction of lanthanide cations in the catalyst formulation slightly reduces the NO_x conversion while increasing at the same time the temperature at which the maximum conversion occurs. In the particular case of the cerium-doped catalysts, a wide range of temperatures exists for which the NO_x conversion is practically unaltered mainly due to both vanadia catalyst and support activity. To a better description of the activity results, experimental data have been fitted by using the kinetic model described by Nam et al. for the SCR reaction of NO_x with NH_3 over V_2O_5/Al_2O_3 catalysts.[43] In this model, by considering the stoichiometry of the NO reduction reaction,

$$6NO + 4NH_3 \rightarrow 5N_2 + 6H_2O$$

and a second-order kinetic,

$$\frac{dC_{NO}}{dt} = -kC_{NO}C_{NH_3}$$

the rate expression in the low-temperature range, where reduc-

TABLE 5: Rate Constants (in $mol_{NO}\ g_{cat}^{-1}\ s^{-1}$) for the SCR Reaction over the Catalysts Studied at the Temperatures Indicated

sample	$k_{200°C} \times 10^{-8}$	$k_{250°C} \times 10^{-8}$	$k_{300°C} \times 10^{-8}$	$k_{350°C} \times 10^{-8}$
0VCeAl	0.8	2.3	5.5	11.0
1VAl		0.1	0.2	0.3
1VCeAl	1.7	3.9	7.5	13.0
5VAl	0.6	1.7	3.8	7.6
5VSmAl	0.4	0.7	1.3	2.0
5VLaAl	0.7	1.8	3.7	6.8
5VCeAl	6.0	11.0	17.0	26.0
10VAl	10.0	29.0	69.0	140.0
10VSmAl	3.5	6.8	12.0	19.0
10VLaAl	2.4	5.6	11.0	19.0
10VCeAl	4.1	7.3	12.0	18.0

TABLE 6: Kinetics Parameters Obtained for the SCR Reaction over V_2O_5/Al_2O_3 and Lanthanide-Doped (La, Sm, and Ce) V_2O_5/Al_2O_3 Catalysts

sample	$E^{\ddagger}$ (kcal mol^{-1})	ln A
0VCeAl	10.5	29.3
1VAl	9.9	25.2
1VCeAl	7.9	27.4
5VAl	9.8	28.4
5VSmAl	6.4	24.3
5VLaAl	8.7	27.4
5VCeAl	5.7	26.3
10VAl	10.3	28.4
10VSmAl	6.6	56.7
10VLaAl	8.0	27.9
10VCeAl	5.7	25.9

tion of NO reaction is dominant over the NH_3 oxidation one, is deduced:

$$k = \frac{3}{2C_{NO}\tau(\alpha - 1)} \ln\frac{\alpha - X_{NO}}{\alpha(1 - X_{NO})}$$

where X_{NO} is the experimental NO conversion, τ the space time,

$$\alpha = \frac{3(C_{NH_3})_o}{2(C_{NO})_o}$$

being $(C_{NH_3})_o$ and $(C_{NO})_o$ the feed concentrations of NH_3 and NO, respectively.

Tables 5 and 6 show the rate constants and kinetic parameters obtained from the Arrhenius plots. The activation energy value of 10% V_2O_5/Al_2O_3 catalysts is similar to that reported for the same solid, in ref 43. The pre-exponential factor is not modified with the vanadium content or with the support nature. The important feature is the difference in the activation energies of the different catalysts. High vanadium loaded lanthanide-doped catalysts present rate constants and activation energy lower than undopped ones. On the other hand, the higher the vanadium content of the solids the higher the rate constant. This is in good agreement with the activity increase observed in V_2O_5 supported catalysts with a V_2O_5 submonolayer coverage[44] when increasing the vanadium loading. On the other hand, this fact is also related with the 10 times higher activity shown by polymeric species than monomeric ones.[45] At low vanadium contents, cerium-doped catalysts have a higher specific activity than the undopped catalyst. This must be explained assuming that at such low vanadium coverage (lower than 0.5 theoretical monolayers) there are left cerium centers exposed on the surface, being the activity observed the result of the superposition of the activities due to vanadium and cerium active sites.

Structure−Activity Relationship. Activation energies for the selective catalytic reduction of NO_x with NH_3 in the presence of O_2 obtained for the undopped V_2O_5/Al_2O_3 catalysts are similar to those described in the literature by Nobe et al.,[46] 9.7 kcal/mol; Eng,[47] 10.4 kcal/mol; and Nam et al.,[43] 12.8 kcal/mol. Increasing the vanadium content in these series of catalysts, a little increase in the activation energy is detected. However, in the series of catalysts doped with lanthanide ions, the activity energy decreases with the vanadium loading. This modified behavior must be correlated with a change in the physicochemical properties of the solids. In this sense, different behaviors as a function of the vanadium content have been observed in the energy position of the vanadium pre-edge peak in the XAS spectra and in the V 2p and Al 2p XPS binding energies, between lanthanide-doped and undopped catalysts. Both measurements have been shown to be related to the V−O bond ionicity,[18] and from here, to the Lewis acido-basicity of the surface.

Characterization results shown above suggest that, at low vanadium contents, vanadium atoms are, essentially, in a regular tetrahedral coordination. Increasing the vanadium content, the percentage of the vanadium species with a higher coordination number and polymerization degree increases, although we can describe the vanadium average polyhedra as an irregular tetrahedra. The presence of lanthanide ions favors the formation of the low coordinated vanadium species. At the high vanadium loading tested, 10%, the formation of lanthanide vanadates $LnVO_4$, is detected by XRD, UV−vis, XPS, and TPR measurements. On the other hand, XAS, XPS, and UV−vis results show an alteration of the electronic density of support cations and supported vanadium ions as a function of the vanadium loading and lanthanide dopant used. The electronic density of the V 3d levels decrease with the vanadium content in the undopped catalysts, while the reverse is true for lanthanide-doped ones. On the other hand, the electronic density of the lanthanide d levels also increase when increasing the vanadium content, leading to, in the case of reducible ions as Ce^{4+}, a modification of the formal oxidation state. From here, the electronic density of the aluminum levels of the lanthanide-doped catalysts must decrease in order to keep the electronic equilibrium of the solid, that means, the Lewis acidity of the catalysts is enhanced. It has been previously shown that the activity in the SCR reaction can be correlated with the Brönsted acidity of the catalysts. If the Lewis acidity of the catalysts is enhanced, the activity in the SCR should decrease.

The experimental relationship between the structure and the activity of the catalysts can be observed in Figure 10. A linear correlation between the XANES V-K-edge prepeak position and the activation energies in the SCR reaction of the catalysts is observed. As we have shown above that the prepeak position is related with the electronic density of the vanadium atoms, this relationship suggests that the activation energy is directly related with the Lewis acidity of the vanadium species, in such a way that the higher the ionicity of the V−O bond, the higher the specific activity of the catalysts.

The low differences in the ionic radii and electronegativity of the lanthanide ions used, produces that the energy levels implied in the Ln-O−V bond are closer one to another. Thus, the V−O bond strengths are also similar and the chemical reactivity of them will be not very different. On the other hand, at high vanadium loading, the formation of surface vanadates on the lanthanide-doped samples is detected by XRD, UV−vis, XPS, and TPR. This can be responsible of the little difference observed in their activity energies with the lanthanide nature.

At low vanadium loading, the low vanadium coverage (lower than 0.5 theoretical monolayers) that allows a support surface exposition explains the differences observed in the rate constants

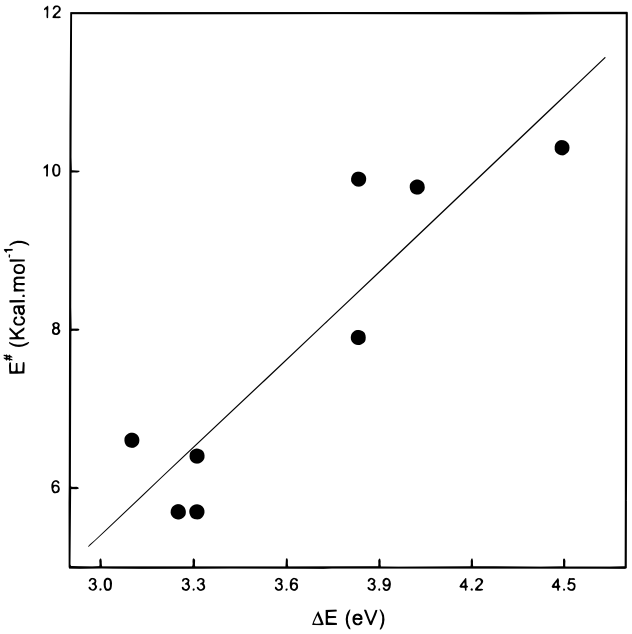

Figure 10. Experimental relationship between the XANES *V−k* pre-edge position and the activation energies in the SCR of NO with NH_3 for the catalysts studied.

in the lanthanide-doped catalysts. In particular, in the case of cerium-doped samples, since the support itself is active in the SCR reaction, due to the existence of the redox pair Ce^{4+}/Ce^{3+}.

Conclusions

When supporting V_2O_5 over Al_2O_3 and lanthanide-doped Al_2O_3 supports, an alteration of the electronic density of all surface ions (aluminum, lanthanide, and vanadium ones) is produced. This alteration depends on the vanadium loading and lanthanide dopant used. The electronic density of the V 3d levels decrease with the vanadium content in the undopped catalysts, while the reverse is true for lanthanide-doped ones. The electronic density of the lanthanide d levels also increases when increasing the vanadium content, leading to, in the case of reducible ions as Ce^{4+}, a modification of the formal oxidation state. To keep the electronic equilibrium of the solid, the electronic density of the aluminum levels of the lanthanide-doped catalysts must decrease. All these alterations produce a change in the Lewis acid−base character of the solids. The activation energy for the SCR reaction increases linearly with the observed XANES V-K-edge prepeak position of the catalysts. As this measurement is related with the electronic density of the vanadium atoms, this relationship suggests that the activation energy is directly related with the Lewis acidity of the vanadium species in such a way that the higher the ionicity of the V−O bond, the higher the specific activity of the catalysts.

Acknowledgment. Financial support for this project has been obtained from Comisión Interministerial de Ciencia y Tecnología (PB92/0665). M. A. Centeno thanks the Junta de Andalucía for the fellowship awarded.

References and Notes

(1) Pârvulescu, V. I.; Grange, P.; Delmon, B. *Catal. Today* **1998**, *46*, 233.
(2) Bosch, H.; Janssen, F. *Catal. Today* **1988**, *2*, 369.
(3) Bond, G. C.; Flamerz Tahir, S. *App. Catal.* **1991**, *71*, 1.
(4) Forzatti, P.; Lietti, L. *Heterog. Chem. Rev.* **1996**, *3*, 33.
(5) Bauerle, G. L.; Wu, S. C.; Nobe, K. *Ind. Eng. Chem. Prod. Res. Dev.* **1978**, *17*, 117.
(6) Centeno, M. A.; Carrizosa, I.; Odriozola, J. A. *Appl. Catal. B* **1998**, *19*, 67.
(7) Capitán, M. J.; Centeno, M. A.; Malet, P.; Carrizosa, I.; Odriozola, J. A.; Márquez, A.; Fernández-Sanz, J. *J. Phys. Chem.* **1995**, *99*, 4655.
(8) Capitán, M. J.; Malet, P.; Centeno, M. A.; Muñoz-Páez, A.; Carrizosa, I.; Odriozola, J. A. *J. Phys. Chem.* **1993**, *97*, 9233.
(9) Odriozola, J. A.; Heinemann, H.; Somorjai, G. A.; Garcia de la Banda, J. F.; Pereira, P. *J. Catal.* **1989**, *119*, 71.
(10) Odriozola, J. A.; Soria, J.; Somorjai, G. A.; Heinemann, H.; Garcia de la Banda, J. F.; Lopez Granados, M.; Conesa, J. C. *J. Phys. Chem.* **1991**, *95*, 240.
(11) Malet, P.; Caballero, A. *J. Chem. Soc., Faraday Trans. 1* **1988**, *84*, 2369.
(12) Sayers, D. E.; Bunker, B. A. In *X-ray Absorption: Principles, Applications and Techniques of EXAFS, SEFAXS and XANES*; Konibsberger, D. C., Prins, R., Eds.; Wiley: New York, 1988.
(13) Tillmanns, E.; Baur, W. H. *Acta Crystallogr. B* **1971**, *27*, 2124.
(14) Malet, P.; Capitán, M. J.; Centeno, M. A.; Odriozola, J. A.; Carrizosa, I. *J. Chem. Soc., Faraday Trans. 1* **1994**, *90*, 2783.
(15) Inomata, M.; Mori, K.; Miyamoto, A.; Murakami, Y. *J. Phys. Chem.* **1983**, *87*, 761.
(16) Niwa, M.; Matsuoka, Y.; Murakami, Y. *J. Phys. Chem.* **1987**, *91*, 4519.
(17) Kozlowski, R.; Pettifer, R.; Thomas, J. M. *J. Phys. Chem.* **1983**, *87*, 5176.
(18) Wong, J.; Lytle, F. W.; Messmer, R. P.; Maylotte, D. H. *Phys. Rev. B* **1984**, *30*, 5596.
(19) Bair, K.; Goddard, W. A., III *Phys. Rev. B* **1980**, *22*, 2767.
(20) Mansour, A.; Cook, J.; Sayers, D. *J. Phys. Chem.* **1984**, *88*, 2330.
(21) Bianconi, A.; Marcelli, A.; Tomellini, M.; Davoli, I. *J. Magn. Magn. Mater.* **1985**, *47*, 209.
(22) Jo, T.; Kotani, A. *Solid State Commun.* **1985**, *54*, 451.
(23) Malterre, D. *Phys. Rev. B* **1991**, *43*, 1391.
(24) Le Normand, F.; Hilaire, L.; Kili, K.; Krill, G.; Maire, G. *J. Phys. Chem.* **1988**, *92*, 2561.
(25) Schraml-Marth, M.; Wokaun, A.; Pohl, M.; Krauss, H. L. *J. Chem. Soc., Faraday Trans. 1* **1991**, *87*, 2635.
(26) Rajadhyaksha, R. A.; Hausinger, G.; Zeilinger, H.; Ramstetter, A.; Schmelz, H.; Knözinger, H. *Appl. Catal.* **1989**, *51(19)*, 67.
(27) Scharf, U.; Schraml-Marth, M.; Wokaun, A.; Baiker, A. *J. Chem. Soc., Faraday Trans.* **1991**, *87*, 3299.
(28) Eon, J. G.; Olier, R.; Volta, J. C. *J. Catal.* **1994**, *145*, 318.
(29) Tanaka, T.; Nishimura, Y.; Kawasaki, S.-I.; Ooe, M.; Funabiki, T.; Yoshida, S. *J. Catal.* **1989**, *118*, 327.
(30) Praline, G.; Koel, B. E.; Mance, R. L.; Lee, H. I.; White, J. H. *J. Electron Spectrosc. Relat. Phenomen.* **1986**, *21*, 17.
(31) Laachir, Ah.; Perrichon, V.; Badri, A.; Lamotte, J.; Catherine, E.; Lavalley, J. C.; El Fallah, J.; Hilaire, L.; Le Normand, F.; Quéméré, E.; Nöel Sauvion, G.; Touret, O. *J. Chem. Soc., Faraday Trans.* **1991**, *87*, 1601.
(32) Kotani, A.; Jo. T.; Okada, K.; Nakano. T.; Okada, M.; Bianconi, A.; Marcelli, A.; Parlebas, J. C. *J. Magn. Magn. Mater.* **1987**, *70*, 28.
(33) Bernal, S.; Calvino, J. J.; Cifredo, A.; Rodriguez-Izquierdo, J. M.; Perrichon, V.; Laarchin, A. *J. Catal.* **1992**, *137*, 1.
(34) Read, J. F. *Can. J. Chem.* **1972**, *50*, 490.
(35) Stobbe-Kreemers, A. W.; Van Leerdam, G. C.; Jacobs, J. P.; Brongersma, H. H.; Scholten, J. J. F. *J. Catal.* **1995**, *152*, 130.
(36) Shyu, S. Z.; Weber, W. H.; Gandhi, H. S. *J. Phys. Chem.* **1988**, *92*, 4964.
(37) Nag, N. K.; Massot, F. E. *J. Catal.* **1990**, *124*, 127.
(38) Wong, W. C.; Nobe, K. *Ind. Eng. Chem. Prod. Res. Dev.* **1986**, *25*, 179.
(39) Singoredjo, L.; Korver, R.; Kapteijn, F.; Moulijn, J. *Appl. Catal. B: Environm.* **1992**, *1*, 297.
(40) Ito, E.; Hultermans, R. J.; Lugt, P. M.; Burgers, M. H. W.; Rigutto, M. S.; Van Bekkum, H.; Van Den Bleek, C. M. *Appl. Catal. B: Environm.* **1994**, *4*, 95.
(41) Yokoyama, C.; Misono, M. *J. Catal.* **1994**, *150*, 9.
(42) Inomata, M.; Miyamoto, A.; Ui, T.; Kobayashi, K.; Murakami, Y. *Ind. Eng. Chem. Prod. Res. Dev.* **1982**, *21*, 424.
(43) Nam, I. S.; Eldridge, J.; Kittrell, J. R. *Ind. Eng. Chem. Prod. Res. Dev.* **1986**, *25*, 186.
(44) Baiker, A.; Dollenmeier, P.; Glinski, M.; Reller, A. *Appl. Catal.* **1989**, *35*, 351.
(45) Went, G. J.; Leu, L.-J.; Bell, A. T. *J. Catal.* **1992**, *134*, 479.
(46) Nobe, K.; Bauerle, G. L.; Wu, S. C. *Final report for EPA by the Engineering School and Applied Sciences*; California University: Los Angeles, 1976.
(47) Eng, C. N. Doctoral Thesis, Massachusetts University, 1980.